Supporting Information

Ferrate(VI) Initiated Oxidative Degradation Mechanisms Clarified by DFT Calculations: A Case for Sulfamethoxazole

Hang Yu,[a] Jingwen Chen,[b,*] Hongbin Xie,[b] Pu Ge,[a] Qingwei Kong,[a] Yi Luo [a,*]

[a] State Key Laboratory of Fine Chemicals, School of Pharmaceutical Science and Technology, Dalian University of Technology, Dalian 116024, China. e-mail: luoyi@dlut.edu.cn

[b] Key Laboratory of Industrial Ecology and Environmental Engineering (MOE), School of Environmental Science and Technology, Dalian University of Technology, Dalian 116024, China. e-mail: jwchen@dlut.edu.cn

17 pages, 14 figures, 10 tables

Table S1. Relative enthalpies (ΔH, kcal mol^{-1}) at MP2//B3LYP level[a] for the complexes forming by SMX and $HFeO_4^-$ and by anionic $SMX^-$and $HFeO_4^-$, respectively.

	SMX	**SMX$^-$**
Complex(1C)	-24.2	28.6

[a] Single point calculations at level of RI-MP2//[ecp(SDD,Def2-SVP/J) for Fe atom, and(Def2-SVPD Def2-SVP/C Def2-SVP/J) (for C, H, O, N, and S atoms)] were performed on the basis of the optimized structures by using the ORCA program[S1].

Table S2. Relative enthalpies (ΔH, kcal mol^{-1}) of the important stationary points involved in the formation of P_a, P_b and P_c, with different functionals.[a]

	B3LYP	M06		B3LYP	M06
1A	-3.2	11.0	**1C**	-2.3	-5.4
TSA$_{1-2}$	10.6	18.4	**TSC$_{1-2}$**	9.8	4.1
TSA$_{3-4}$	28.3	39.1	**TSC$_{2-3}$**	22.1	10.5
1B	-2.1	-6.1	**TSD$_{2-3}$**	13.9	7.1
TSB$_{1-2}$	20.1	4.9	$\Delta H^{\ddagger}$(C)	24.4	15.9
$\Delta H^{\ddagger}$(A)	31.5	39.1	$\Delta H^{\ddagger}$(D)	16.1	12.5
$\Delta H^{\ddagger}$(B)	22.2	11.0			

[a]Calculated at the level of B3LYP/BSII(IEFPCM)//B3LYP/BSI and M06/BSII(IEFPCM)//M06/BSI, respectively.

Table S3. Relative enthalpies (ΔH, kcal mol^{-1}) of the important stationary points in the formation of P_a, P_b and P_c, which were calculated with different strategies.

	Gas[a]	PCM1[b]	SMD[c]	PCM2[d]		Gas	PCM1	SMD	PCM2
1A	-3.2	-3.8	-2.5	-7.3	**1C**	-2.3	-2.5	-0.9	-2.1
TSA$_{1-2}$	10.6	6.9	13.4	9.3	**TSC$_{1-2}$**	9.8	10.7	8.5	11.8
TSA$_{3-4}$	28.3	22.5	26.5	22.0	**TSC$_{2-3}$**	22.1	22.6	25.0	22.9
1B	-2.1	-3.7	-0.8	-4.0	**TSD$_{2-3}$**	13.9	13.6	10.9	14.1
TSB$_{1-2}$	20.1	19.6	16.2	17.4	$\Delta H^{\ddagger}$(C)	24.4	25.1	25.9	25.0
$\Delta H^{\ddagger}$(A)	31.5	26.3	29.0	29.3	$\Delta H^{\ddagger}$(D)	16.1	16.1	11.8	16.2
$\Delta H^{\ddagger}$(B)	22.2	24.3	17.0	21.4					

[a] Calculated at the level of B3LYP/BSII(IEFPCM)//B3LYP/BSI.

[b] Calculated at the level of B3LYP/BSII(IEFPCM)//B3LYP/BSI(IEFPCM).

[c] Calculated at the level of B3LYP/BSII(SMD)//B3LYP/BSI(SMD).

[d] Calculated at the level of B3LYP/BSII(IEFPCM)//B3LYP/BSII(IEFPCM)

Table S4. Calculated Gibbs free energies (kcal mol^{-1}) of stationary points shown in Figure 2a

Stationary points	ΔG	Stationary points	ΔG
SMX + $HFeO_4^-$	0.0	SMX + $HFeO_4^-$ + H_2O	0.0
^{3}1A	7.2	**^{3}3A**	26.9
^{3}TSA$_{1-2}$	23.5	**^{3}TSA$_{3-4}$**	52.1
^{3}2A	19.4	**^{3}4A**	27.8

Table S5. Calculated Gibbs free energies (kcal mol^{-1}) of stationary points shown in Figure 2b

Stationary points	ΔG	Stationary points	ΔG
SMX + $HFeO_4^-$	0.0	**^{5}TSB$_{3-4}$**	24.2
^{3}1B	10.0	**^{5}4B**	16.3
^{3}TSB$_{1-2}$	35.6	**^{5}TSB$_{4-5}$**	18.5
^{3}2B	17.4	**^{5}5B**	2.7
^{3}TSB$_{2-3}$	23.7	P_a + $HFeO_3^-$	0.2
^{3}3B	20.6		

Table S6. Calculated Gibbs free energies (kcal mol^{-1}) of stationary points shown in Figure 3

Stationary points	ΔG	Stationary points	ΔG
SMX + $HFeO_4^-$	0.0	**^{3}TSD$_{3-4}$**	25.6
^{3}1C	7.2	**^{5}4D**	-11.6
^{3}TSC$_{1-2}$	20.8	**^{5}TSD$_{4-5}$**	-5.7
^{5}2C	16.3	**^{5}5D**	-26.0
^{5}TSC$_{2-3}$	32.9	**^{7}TSD$_{5-6}$**	-23.3
^{5}3C	3.9	**^{7}6D**	-26.8
SMX N-radical + $H_2Fe(V)O_4^{\cdot-}$	3.6	P_c + $H_3Fe(II)O_3^-$	-33.9

^{5}3D	18.2

Table S7. Calculated Gibbs free energies (kcal mol^{-1}) of stationary points shown in Figure 4

Stationary points	ΔG	Stationary points	ΔG
P_c + $HFeO_4^-$	0.0	P_c + $HFeO_4^-$ + H_2O	0.0
^{3}7E1	11.3	**^{3}7E2**	17.5
^{3}TSE1$_{7\text{-}8}$	22.2	**^{3}TSE2$_{7\text{-}8}$**	44.2
^{3}8E1	-2.0	**^{5}8E2**	8.6
^{3}TSE1$_{8\text{-}9}$	-2.4		
^{5}9E1	-16.8		

Table S8. Relative enthalpies (ΔH, kcal mol^{-1}) of various states of Fe species in oxidation process

Fe Species	Singlet	Doublet	Triplet	Quartet	Quintet
$HFe(VI)O_4^-$	22.7	/	0.0	/	14.74
$H_2Fe(V)O_4^-$	/	1.3	/	0.0	/
$HFe(IV)O_3^-$	16.2	/	1.0	/	0.0

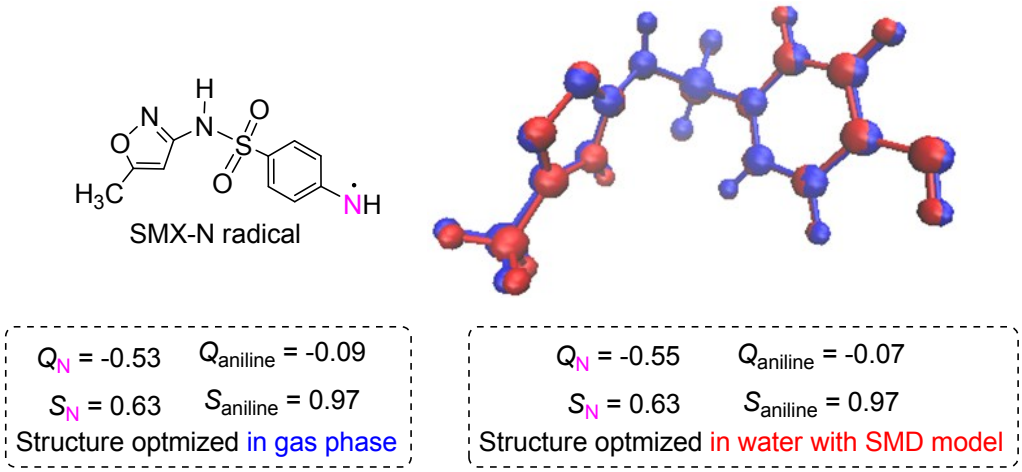

Fig. S1. The structures, natural charge (Q), and spin density (S) for aniline moiety and N atom of aniline moiety (in pink) of SMX-N radical optimized in gas (structure in blue) and water solution (SMD model, structure in red) phases. The spin population on aniline moiety containing its N atom is 0.97 in both gas-phase and solution, suggesting that the unpaired

electron resides on the aniline moiety.

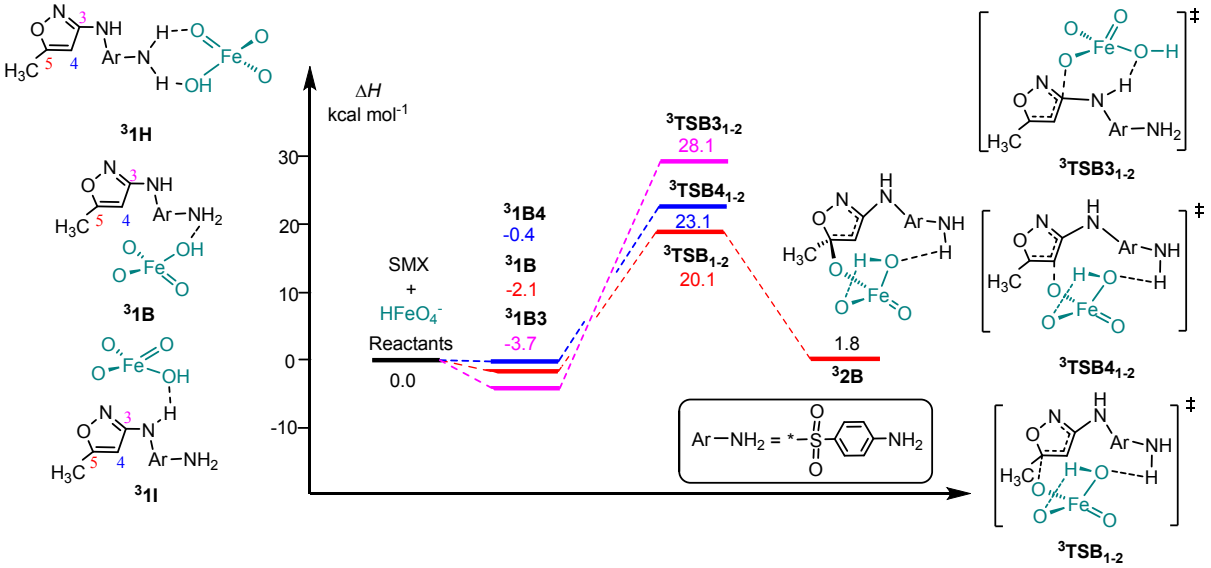

Fig. S2. Computed enthalpy profiles (kcal mol^{-1}) for the nucleophilic attack to different sites of the isoxazole moiety of SMX during the ferrate(VI)-mediated oxidation of the isoxazole unit (The enthalpy values given are relative to the corresponding reactants. The left-superscript in the labeling of the stationary points denotes the corresponding spin multiplicity. The sign of negative charge is not shown)

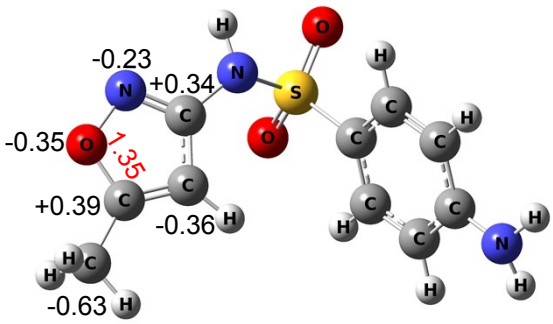

Fig. S3. Atomic NBO charges of the isoxazole moiety (in black) and the length of C_5–O_1 bond (distances is Å, shown in red) in SMX

Table S9. Relative enthalpies (ΔH, kcal mol^{-1}) of the important stationary points in the formation of P_a, which were carried out based on IEFPCM with different solvent cavities in single-point energy calculations

	UFF	Bondi[a]
1A	-3.2	-0.5
TSA$_{1-2}$	10.6	13.8
TSA$_{3-4}$	28.3	30.4
1B	-2.1	0.6
TSB$_{1-2}$	20.1	27.1
$\Delta H^{\ddagger}$(path A)	**31.5**	**30.4**
$\Delta H^{\ddagger}$(path B)	**22.2**	**27.1**

[a] Being in agreement with the UFF result, the results derived from Bondi solvent radii also suggest that Path B is more favorable than Path A, although the Bondi radii results in smaller difference in energy barrier (3.5 *vs.* 9.3 kcal mol^{-1}).

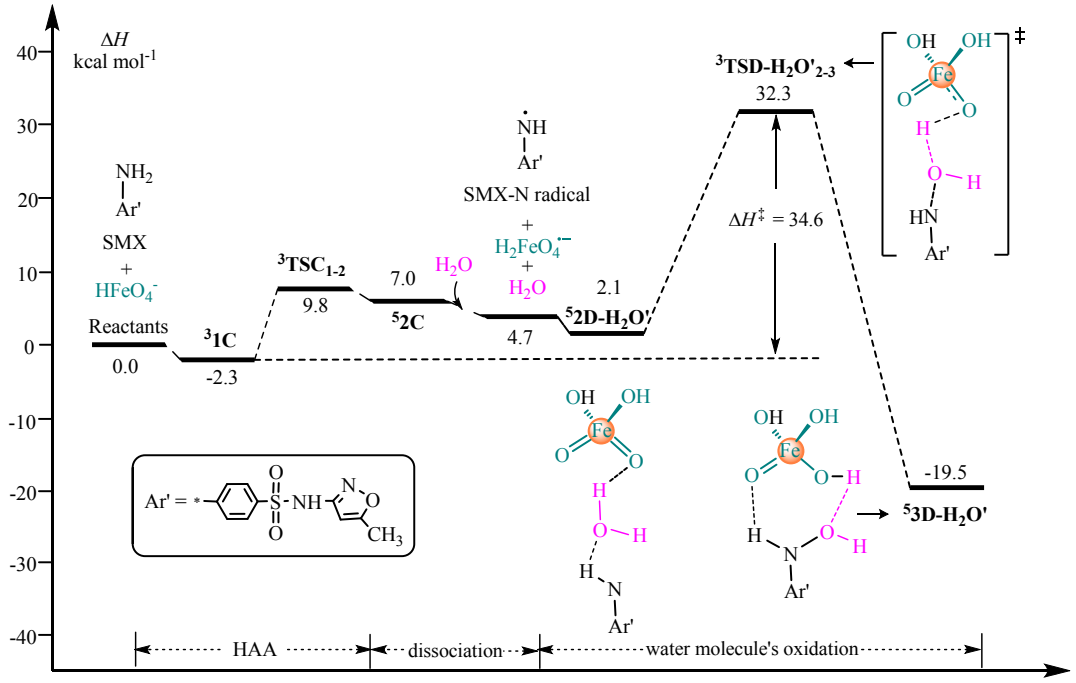

Fig. S4. Computed enthalpy profiles (kcal mol^{-1}) of the formation of hydroxylamine moiety, in which water molecule acted as oxygen atom donor (The enthalpy values given are relative to

the corresponding reactants. The left-superscript in the labeling of the stationary points denotes the corresponding spin multiplicity. The sign of negative charge is not shown)

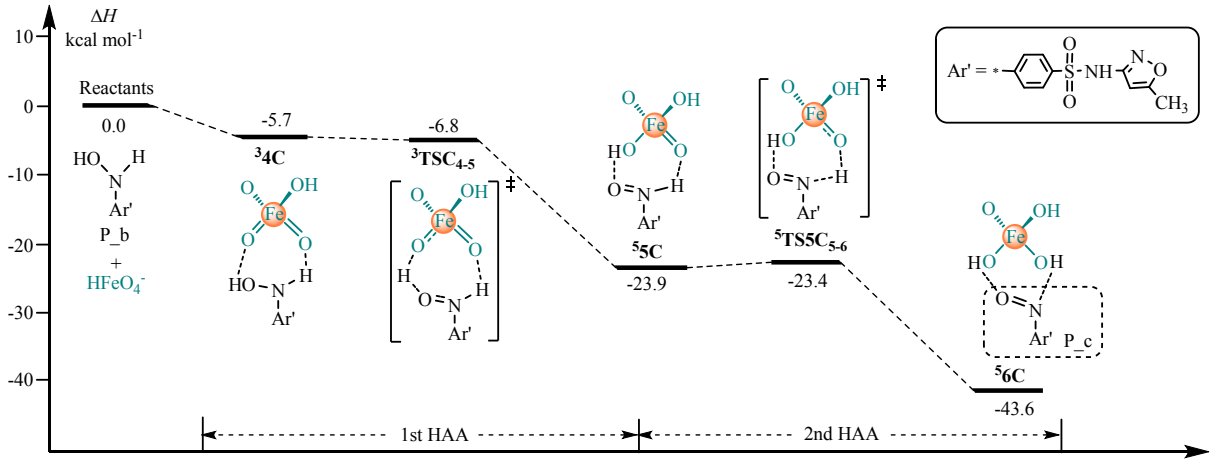

Fig. S5. Computed enthalpy profiles (kcal mol^{-1}) for the conversion of P_b to P_c (The enthalpy values given are relative to the corresponding reactants. The left-superscript in the labeling of the stationary points denotes the corresponding spin multiplicity. The sign of negative charge is not shown)

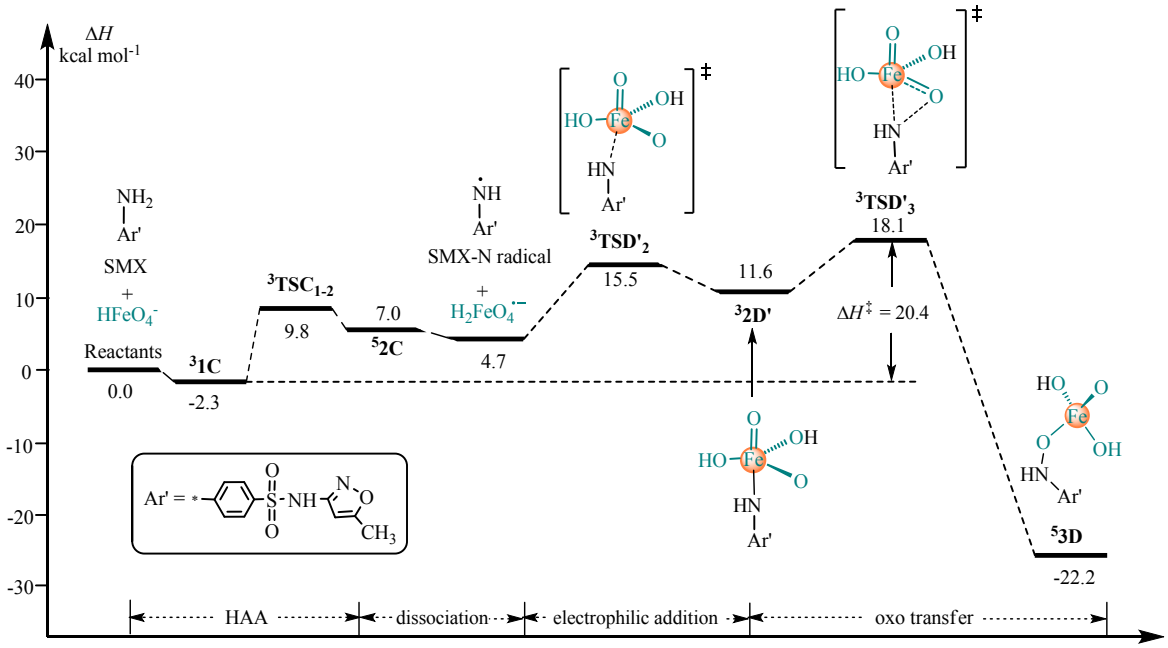

Fig. S6. Computed enthalpy profiles (kcal mol^{-1}) of the formation of Fe–O bond by an imidoiron intermediate (The enthalpy values given are relative to the corresponding reactants. The left-superscript in the labeling of the stationary points denotes the corresponding spin multiplicity. The sign of negative charge is not shown)

Effects of explicit water molecule

To further consider solvation effect of water, besides the usage of implicit solvation model, the involvement of water molecule as explicit solvent molecule was also considered for calculations of reaction pathways.

It is noted that the involvement of two or more water molecules as explicit solvent molecules to interact with substrates was previously found to have no significant effect on the energy barrier in comparison with the case of one water molecule,[S2,S3] only one water molecule was considered in the current study. As shown in Fig. S7, the results show that the involvement of a water molecule in favorable pathways has a variation of no more than 2 kcal mol^{-1}, compared with that without coordination of a water molecule. This suggests explicit solute-solvent interactions have no significant influences in the current theoretical results for ferrate(VI)-mediated oxidation of SMX. It deserves mentioning that attempts to locate the complex of $HFeO_4^-$ with one or two water molecules through direct interaction between O atom of water and the Fe atom were fruitless, possibly due to the steric effect.

It is also noteworthy that one explicit water molecule has been considered for coordination to SMX via potential hydrogen bonds. Six complexes have been computationally located, and the structure with double hydrogen bonds between water and the isoxazole as well as $HN{-}SO_2$ moieties (**A**) is most stable among these complexes (Fig. S8). This stable structure has been further chosen to analyze the rate-determining steps for formation of P_a, P_b, and P_c. The results indicate that the activation enthalpies don't significantly change in comparison with the case of the absence of explicit water molecule (see Table S10).

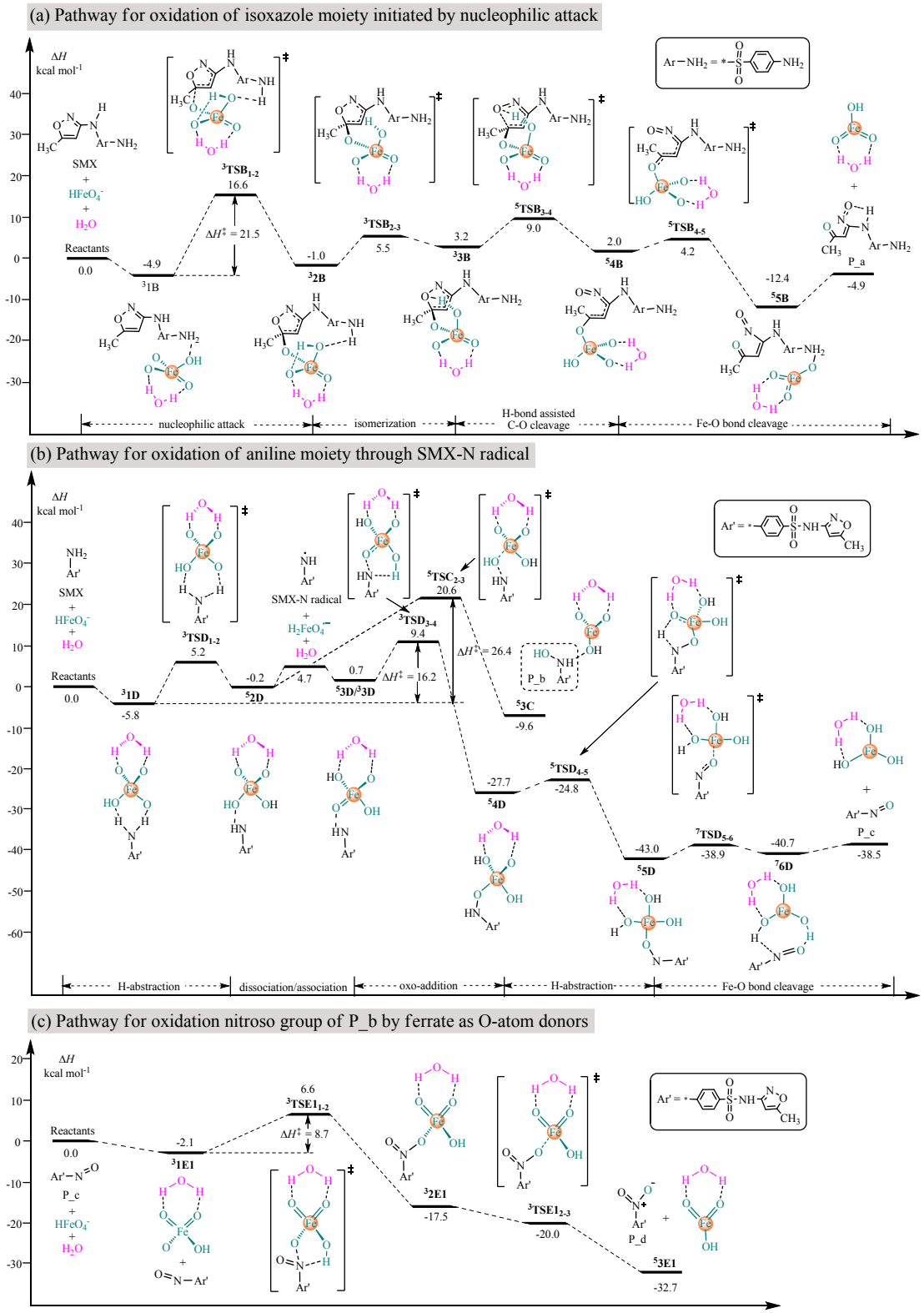

Fig. S7. Computed enthalpy profiles (kcal mol^{-1}) of all favorable pathways involved a water molecule interacted with the Fe species (The enthalpy values given are relative to the corresponding reactants. The left-superscript in the labeling of the stationary points denotes the corresponding spin multiplicity. The sign of negative charge is not shown).

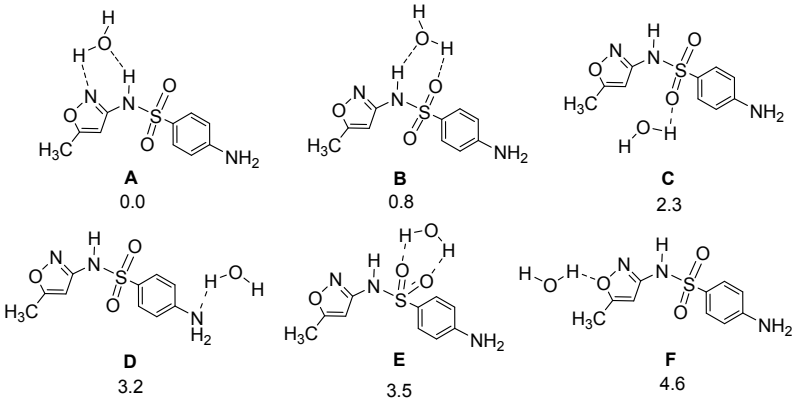

Fig. S8. Structures and relative enthalpies of water-SMX complexes. The enthalpies relative to structure **A** were shown under the structure.

Table S10. Relative enthalpies of the important stationary points and energy barriers for the formation of P_a, P_b, and P_c. The enthalpies were relative to **A** (with water coordinating to SMX, see Fig. S8) and $HFeO_4^-$ or SMX (without water) and $HFeO_4^-$.

Stationary points	**SMX**	**A**	Energy barriers	**SMX**	**A**
1B	-2.1	-0.4			
TSB$_{1-2}$	20.1	21.8	$\Delta H^{\ddagger}$(B)	22.2	22.1
1C	-2.3	-1.6			
TSC$_{2-3}$	22.1	23.6	$\Delta H^{\ddagger}$(C)	24.4	25.2
TSD$_{2-3}$	13.9	16.3	$\Delta H^{\ddagger}$(D)	16.1	17.7

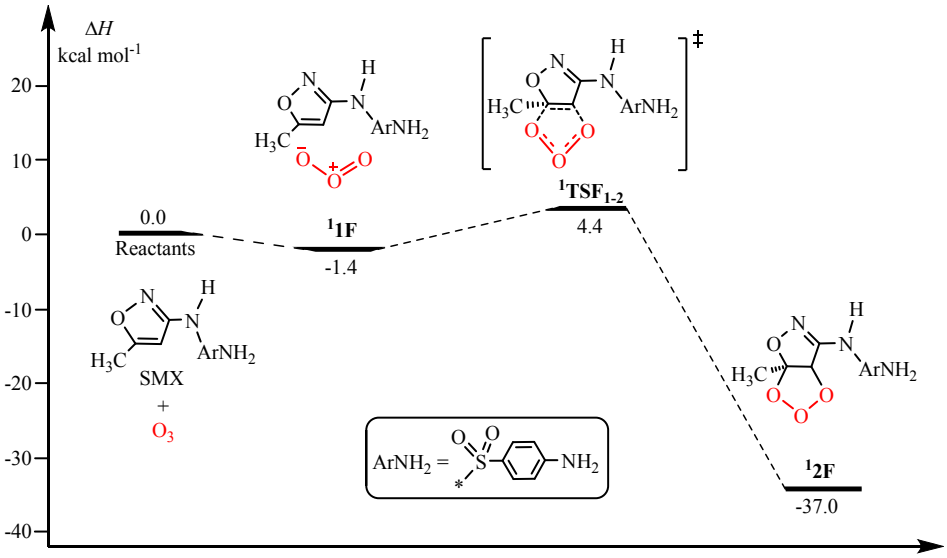

Fig. S9. Computed enthalpy profiles (kcal mol^{-1}) for ozone-mediated oxidation pathways of the isoxazole moiety of SMX (The enthalpy values given are relative to SMX and O_3. The left-superscript in the labeling of the stationary points denotes the corresponding spin multiplicity)

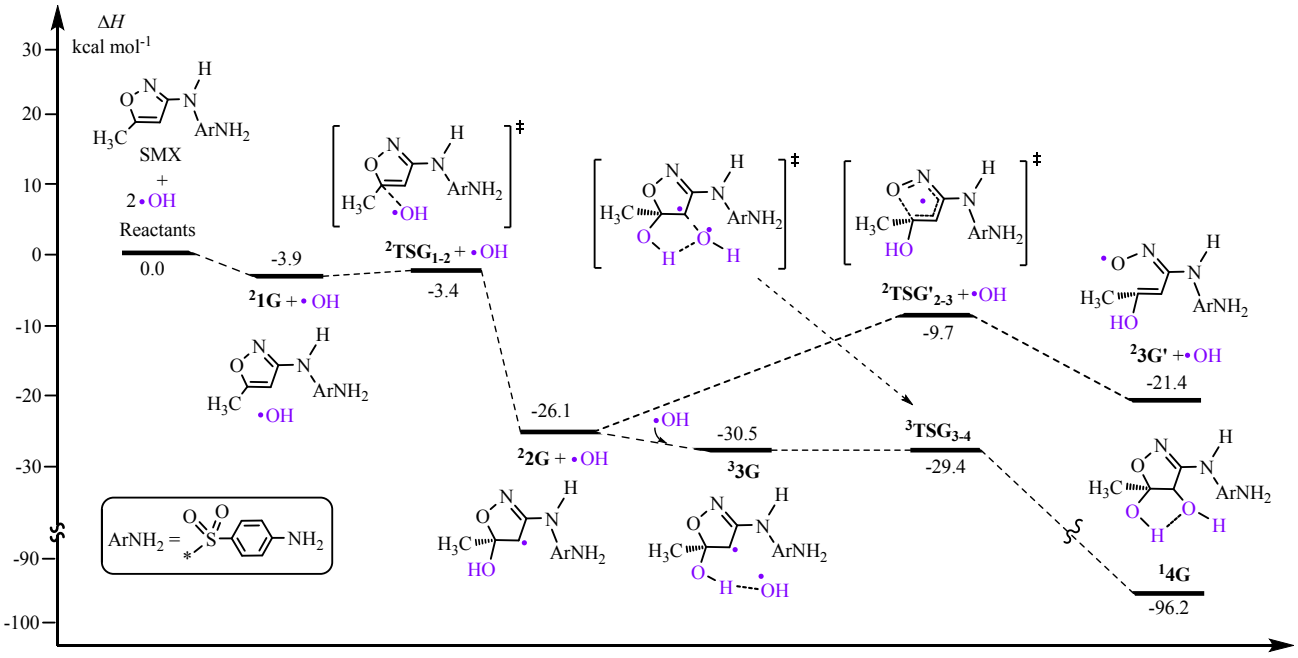

Fig. S10. Computed enthalpy profiles (kcal mol^{-1}) for ·OH-mediated oxidation pathways of the isoxazole moiety of SMX (The enthalpy values given are relative to SMX and two molecular ·OH. The left-superscript in the labeling of the stationary points denotes the corresponding spin multiplicity)

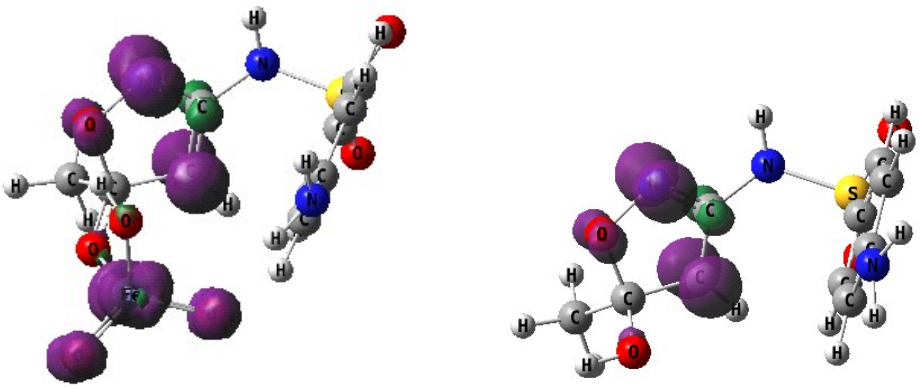

^{3}**3B** ^{2}**2G**

Fig. S11. Spin density distribution on ^{3}**3B** and ^{2}**2G** (isovalue of 0.01)

In the case of SMX degradation by persulfate assisted micrometric Fe(0).

SMX degradation by persulfate assisted Fe(0) was proposed by Ghauch, A. et al. (ref. 28), and a ring-opening (N–O bond cleavage) reaction of isoxazole moiety through radical anion formation ($SMX^{\bullet-}$) and radical cation formation ($SMX^{\bullet+}$) was reported. In our calculation, there is little spin density distribution (0.01 ~ 0.07) on the isoxazole moiety of $SMX^{\bullet-}$ or $SMX^{\bullet+}$. Attempts to locate transition state for cleavage of N–O bond in $SMX^{\bullet-}$ or $SMX^{\bullet+}$ were fruitless. However, the charge analysis of $SMX^{\bullet-}$ indicates that N atom of isoxazole moiety has strong nucleophilicity. Since the reaction occurs in acidic medium, the N atom could easily capture H^+ to form $SMXH^{\bullet}$. The spin density on isoxazole moiety of $SMXH^{\bullet}$ is 0.91, indicating that the unpaired electron was distributed on the isoxazole moiety. The energy barrier for the N–O bond cleavage of isoxazole moiety of $SMXH^{\bullet}$ is 2.6 kcal mol^{-1}, indicating a feasible ring-opening reaction. This result as another example shows that the electron delocalization is crucial for the ring-opening of isoxazole moiety of SMX.

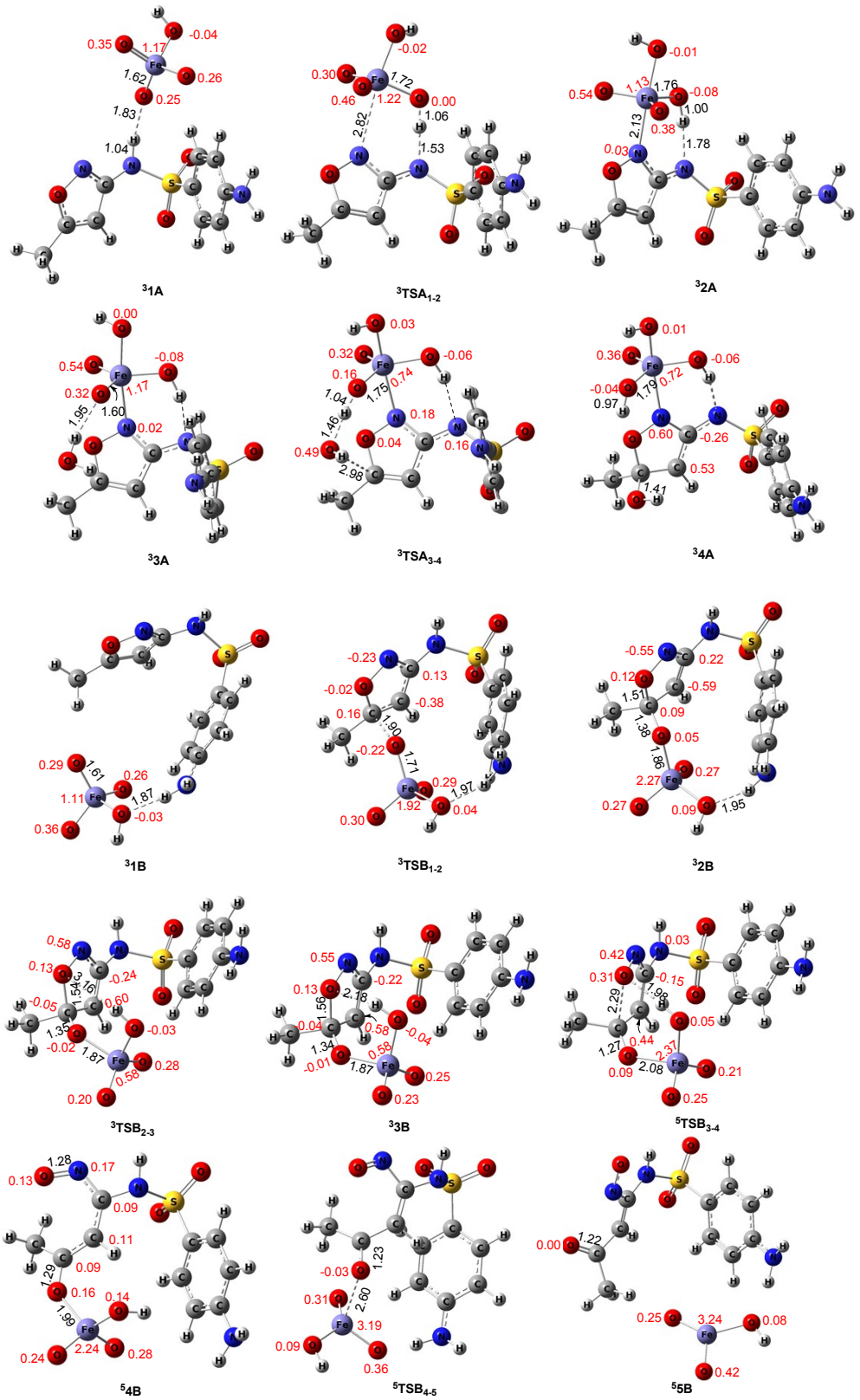

Fig. S12. Optimized geometrical parameters (distances is Å, shown in black) and spin densities (in red) of intermediates and transition states during the ferrate(VI)-mediated oxidation of isoxazole moiety.

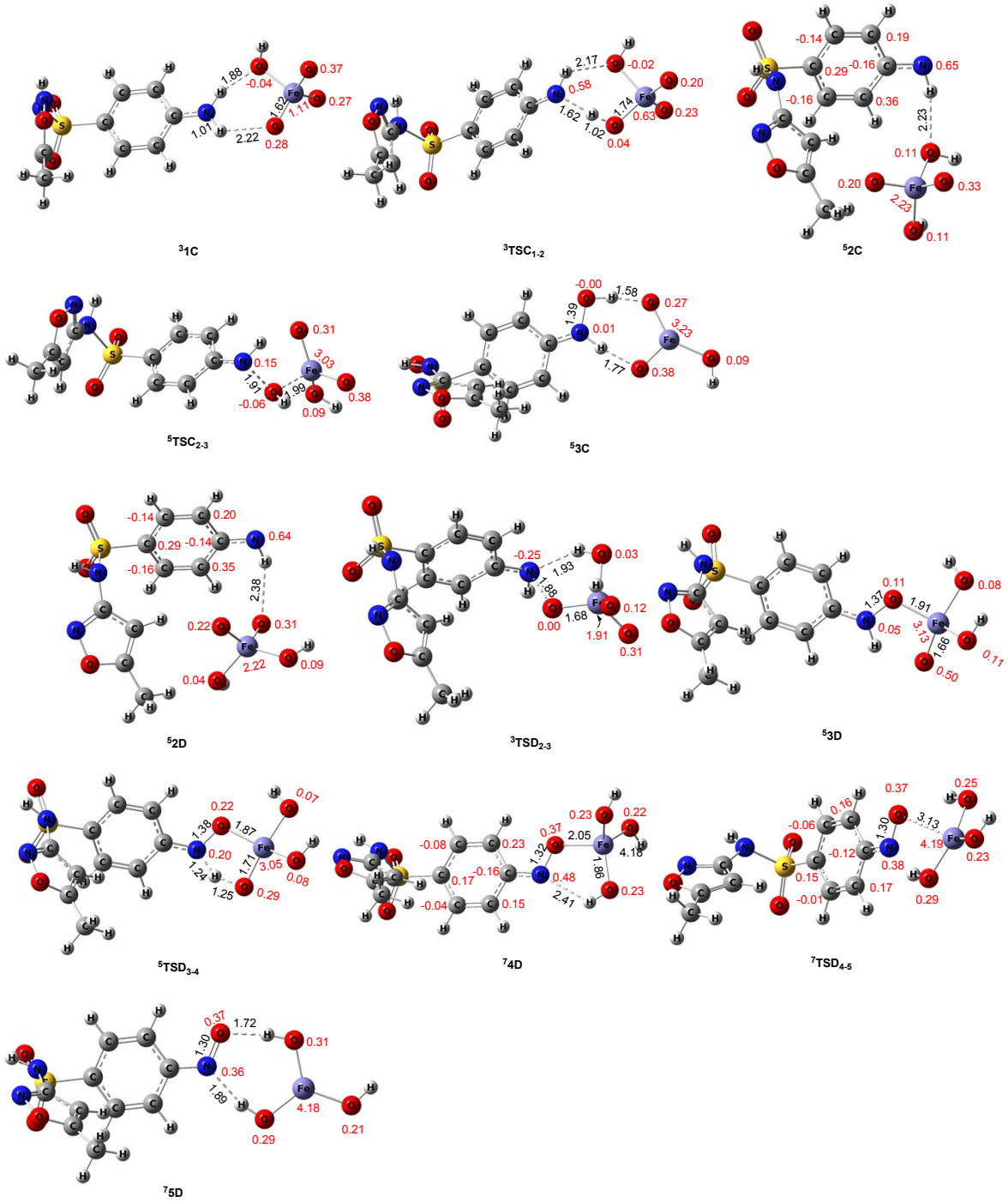

Fig. S13. Optimized geometrical parameters (distances is Å, shown in black) and spin densities (in red) of intermediates and transition states during the ferrate(VI)-mediated oxidation of aniline moiety to yield P_b and P_c.

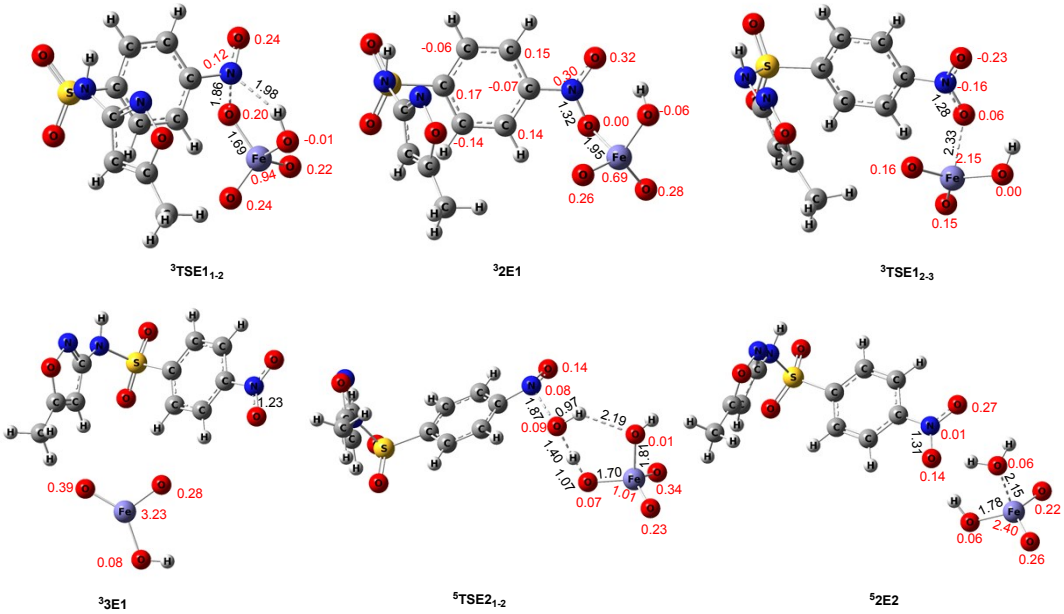

Fig. S14. Optimized geometrical parameters (distances in Å, shown in black) and spin densities (in red) of intermediates and transition states involved in the ferrate(VI)-mediated conversion of P_c to P_d.

REFERENCES

S1. F. Neese, The ORCA program system. *WIREs Comput. Mol. Sci.*, 2012, **2**, 73–78.

S2. H. Zhang, H. Xie, J. Chen and S. Zhang, *Environ. Sci. Technol.*, 2015, **49**, 1552–1558.

S3. Y. Liang, H. Zhou and Z. Yu, *J. Am. Chem. Soc.*, 2009, **131**, 17783–17785.